Photoactivatable drugs for nicotinic optopharmacology

Sambashiva Banala[1,8], Matthew C Arvin[2,8], Nicholas M Bannon[3], Xiao-Tao Jin[2], John J Macklin[1], Yong Wang[2], Can Peng[2], Guiqing Zhao[2], John J Marshall[4], Kyle R Gee[5], David L Wokosin[4], Veronica J Kim[2], J Michael McIntosh[6], Anis Contractor[3,4], Henry A Lester[1,7], Yevgenia Kozorovitskiy[3], Ryan M Drenan[2,9] & Luke D Lavis[1,9]

Photoactivatable pharmacological agents have revolutionized neuroscience, but the palette of available compounds is limited. We describe a general method for caging tertiary amines by using a stable quaternary ammonium linkage that elicits a red shift in the activation wavelength. We prepared a photoactivatable nicotine (PA-Nic), uncageable via one- or two-photon excitation, that is useful to study nicotinic acetylcholine receptors (nAChRs) in different experimental preparations and spatiotemporal scales.

Photoactivatable (caged) compounds remain the primary tools for modulation of native proteins with high spatiotemporal resolution. Uncaging of ligands for glutamate and GABA receptors enabled seminal optopharmacology studies on the biophysics and subcellular location of functional proteins in complex biological environments[1–3], but caged ligands targeting other receptors remain rare. We developed a general strategy for preparing photoactivatable drugs through alkylation of tertiary nitrogen atoms to form photolabile quaternary linkages. Our photoactivatable nicotine (PA-Nic) has ideal chemical and spectroscopic properties for use in investigations of endogenous nAChRs in brain tissue.

Many pharmacological agents cannot be caged via standard strategies because they lack obvious attachment sites (e.g., CO_2H, OH, NH) for photolabile groups. A canonical example of a previously uncageable drug is the nAChR agonist nicotine (compound **1**; **Fig. 1a**), but other such compounds exist, including the AChR agonists cevimeline (**2**), PNU-282,987 (**3**), milameline (**4**), and oxotremorine (**5**), as well as the opioid fentanyl (**6**) and the selective serotonin-reuptake inhibitor escitalopram (**7**; **Fig. 1b**). A shared feature of these compounds is a tertiary nitrogen, a common motif in many pharmacological agents that is often critical for biological activity (**Supplementary Note 1**). We envisioned a general caging strategy involving covalent attachment of a coumarin[4–6] cage to form a quaternary ammonium salt. Quaternization has been used to create photoactivatable tertiary amines such as polymer initiators[7], amino acids[8], mustards[9], and anticancer agents[10], but such compounds have not been reported in biological experiments. We applied this strategy to nicotine (**1**), and alkylated with coumarin (**8**) to obtain PA-Nic (**9**; **Fig. 1a**). PA-Nic releases nicotine when exposed to UV illumination (365 nm) with an uncaging quantum yield (Φ_u) of 0.74%, and generates coumarins **10** and **11** as byproducts, which suggests a radical-mediated photolytic mechanism (**Fig. 1a**,**c**, **Supplementary Fig. 1a**, **Supplementary Note 1**). The relatively low Φ_u value for PA-Nic is compensated, in part, by a high extinction coefficient (ε = 17,400 M^{-1} cm^{-1}). In our study PA-Nic showed excellent dark stability in aqueous solution (**Fig. 1d**), and formation of the quaternary center at the 4-position of the coumarin elicited an unexpected ~15-nm red shift in the absorption maxima of the coumarin cage (λ_{max} = 404 nm; **Fig. 1e**), thus matching it to ~400-nm light sources. We then applied this strategy to prepare quaternary ammonium photoactivatable derivatives of compounds **2**–**7**, which all showed photoconversion with similar Φ_u values, excellent dark stability, red-shifted λ_{max}, high ε, and the same coumarin byproducts (**Supplementary Fig. 1b**–**k**, **Supplementary Note 1**). We also confirmed that a quaternary center is necessary for the shift in λ_{max} (**Supplementary Fig. 1l**,**m**).

With the generality of this caging strategy established, we focused on PA-Nic (**9**) by comparing it to the previously described photoactivatable ruthenium bis(bipyridine)–nicotine complex[11] (RuBi-Nic; **20**; **Supplementary Fig. 2a**). We prepared mouse brain slices containing the medial habenula (MHb), neurons of which express high numbers of nAChRs[12], corelease acetylcholine (ACh) and glutamate[13], and regulate affective behavior and nicotine withdrawal[14] (**Supplementary Fig. 2b**–**d**). Light flashes (1 s; 390 ± 10 nm) evoked robust nicotinic currents with PA-Nic (80 μM; **Fig. 1f**), but RuBi-Nic elicited much smaller currents with longer photolysis (15 s; 470 nm) and proved unstable (**Supplementary Fig. 2e**,**f**). In addition, PA-Nic photolysis was negligible at 470 nm and 560 nm (100 ms; 0.06 mW mm^{-2}; **Supplementary Fig. 2g**), which allows for the use of other fluorophores or light-activated effectors. The main photochemical by-product of PA-Nic photolysis (**10**) was inert at nAChRs;

[1]Janelia Research Campus, Howard Hughes Medical Institute, Ashburn, Virginia, USA. [2]Department of Pharmacology, Northwestern University Feinberg School of Medicine, Chicago, Illinois, USA. [3]Department of Neurobiology, Weinberg School of Arts and Sciences, Northwestern University, Evanston, Illinois, USA. [4]Department of Physiology, Northwestern University Feinberg School of Medicine, Chicago, Illinois, USA. [5]Molecular Probes, Thermo Fisher, Eugene, Oregon, USA. [6]George E. Wahlen Veterans Affairs Medical Center and Departments of Psychiatry and Biology, University of Utah, Salt Lake City, Utah, USA. [7]Division of Biology and Biological Engineering, California Institute of Technology, Pasadena, California, USA. [8]These authors contributed equally to this work. [9]These authors jointly directed this work. Correspondence should be addressed to L.D.L. (lavisl@janelia.hhmi.org) or R.M.D. (drenan@northwestern.edu).

RECEIVED 26 SEPTEMBER 2017; ACCEPTED 26 FEBRUARY 2018; PUBLISHED ONLINE 26 MARCH 2018; DOI:10.1038/NMETH.4637

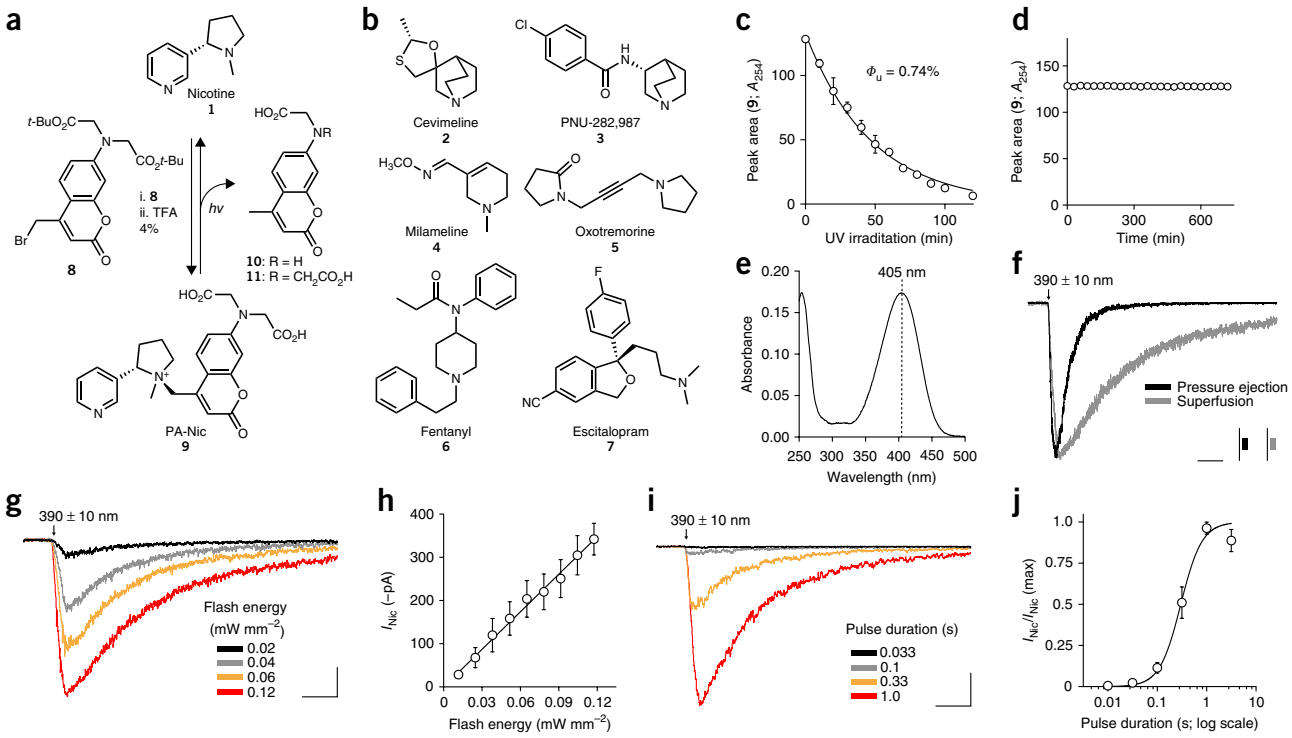

Figure 1 | Development of PA-Nic and its utility for improved pharmacological studies of native nAChRs. (**a**) Chemical structure of nicotine (**1**) and the synthesis and photolysis of PA-Nic (**9**). (**b**) Chemical structures of uncageable drug compounds **2**–**7**. (**c**) A plot of mean HPLC chromatogram peak area versus UV irradiation time (365 nm), which provides the uncaging quantum yield (Φ_u). The solid line shows the exponential fit; error bars indicate ±s.d. n = 2 independent samples. (**d**) Data from a representative dark stability experiment with PA-Nic (**9**); n = 3 independent samples. (**e**) Absolute absorption spectrum of PA-Nic (**9**; 10 µM); representative results from one of three independent samples. (**f**) Light-evoked currents after PA-Nic epi-illumination photolysis. Shown are voltage-clamp traces from individual MHb neurons obtained with different methods of PA-Nic application (results shown are from one experiment representative of >10 independent experiments with similar results). Photolysis: 1-s pulse, 0.12 mW mm^{-2}. Scale: 2.5 s, 100 pA (gray) or 150 pA (black). (**g**–**j**) Controllable nicotine uncaging via PA-Nic epi-illumination photolysis. (**g**) Voltage-clamp traces from an MHb neuron after light pulses (1 s) of varying intensity. Scale: 2.5 s, 75 pA. Results shown are from 1 experiment representative of 4 independent experiments. (**h**) Resulting photochemical dose–response relation for peak currents ($y = 2.876x + 2.1$; $R^2 = 0.9921$). Shown is the mean (n = 9 cells from 6 mice) peak of light-activated currents plotted against the input flash intensity. (**i**) Voltage-clamp traces during light pulses (0.12 mW mm^{-2}) of varying duration applied to an MHb neuron. Scale: 2.5 s, 250 pA. Results shown are from 1 experiment representative of 5 independent experiments. (**j**) Graphical analysis of the summary pulse duration data in **i**. The Hill equation was fitted to the mean data (n_H (Hill slope) = 2.0; duration at half-maximum = 0.3 s; R^2 = 0.928) from n = 5 cells from 3 mice. Error bars in **h**,**j** indicate ±s.e.m.

PA-Nic itself exhibited no nAChR-antagonist properties, and our preparations of PA-Nic were devoid of free nicotine (**Supplementary Fig. 2h**–**k**). PA-Nic photolysis currents were eliminated by an nAChR-antagonist cocktail and reversed at approximately +2 mV (**Supplementary Fig. 2l**–**n**). Pressure-ejection application of nicotine and ACh provided calibration for PA-Nic photolysis currents (**Supplementary Fig. 2o**,**p**). Epi-illumination flashes elicited responses that increased in amplitude with increasing flash energy and flash duration (**Fig. 1g**–**j**). Thus, light-evoked nicotine release allowed the generation of complete photochemical concentration–response relations in neurons, which is an advantage over existing drug-application approaches.

Next, we determined whether PA-Nic could be used during two-photon laser scanning microscopy (2PLSM) and two-photon photolysis. The two-photon fluorescence action cross-section (δ_f; Online Methods) spectrum of PA-Nic was distinct from that of GCaMP6f (**Supplementary Fig. 3a**). We measured the two-photon uncaging action cross-section (δ_u) as 0.094 Goeppert–Mayer units (GM) at the maximal two-photon absorption (810 nm) and as 0.059 GM and 0.025 GM at the commonly used 760-nm and 720-nm photolysis wavelengths, respectively[4] (**Supplementary Fig. 3b**,**c**, Online Methods, **Supplementary Note 1**). These values are similar to those for the widely used 4-methoxy-7-nitroindolinyl (MNI)-glutamate (δ_u = 0.06 GM at 730 nm)[1]. PA-Nic (100 µM) photostimulation (720 nm) evoked stable inward currents, and no responses were evoked at 760–900 nm in the absence of PA-Nic (**Supplementary Fig. 3d**,**e**). At 760 nm, two-photon photolysis amplitudes increased with longer pulse durations at a fixed laser power or with increasing laser power at a fixed pulse duration (**Supplementary Fig. 3f**,**g**).

To study nAChRs in cellular compartments, we visualized MHb neuronal morphology with 2PLSM and uncaged nicotine with perisomatic one-photon laser pulses (405 nm, ~1-µm spot diameter). After confirming that moderate laser powers (1–2.5 mW, 50 ms) did not elicit currents in the absence of PA-Nic, we identified suitable photostimulation parameters by measuring the relationship between evoked currents and laser power and pulse duration (**Supplementary Fig. 3h**–**m**). PA-Nic

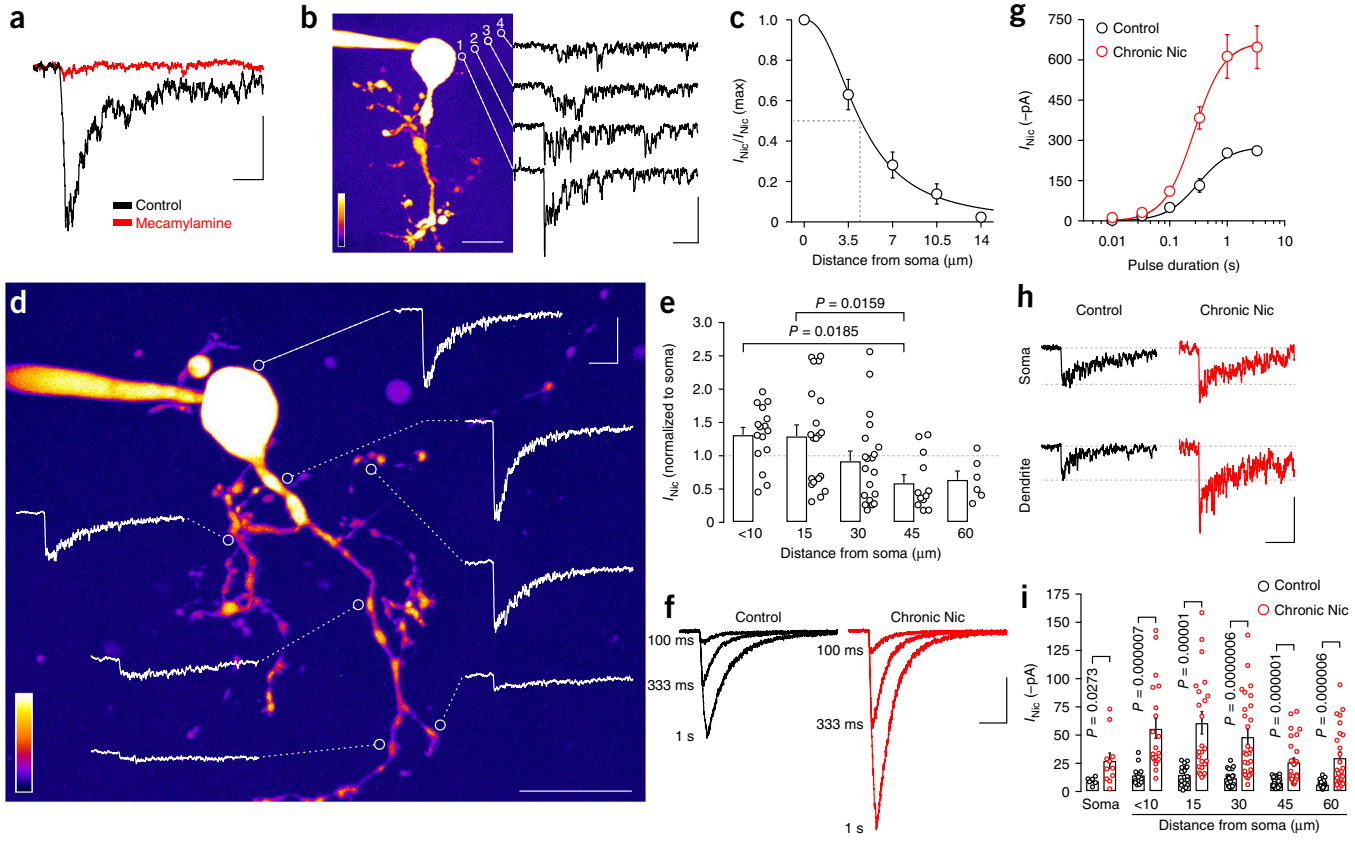

Figure 2 | PA-Nic enables subcellular mapping of nAChRs after chronic nicotine treatment. (**a**) PA-Nic uncaging and mecamylamine antagonism. Nicotine was uncaged in an ~1-µm perisomatic spot with a 405-nm laser pulse (10 ms, 2.9 mW). Voltage-clamp currents before (black trace; results shown are from 1 experiment representative of >10 independent experiments) and 10 min after (red trace; single experiment) mecamylamine (10 µM) superfusion are shown. Scale: 50 ms, 100 pA. (**b**,**c**) Lateral spread of uncaged nicotine, estimated electrophysiologically. (**b**) A representative 2PLSM image of an MHb neuron. Nicotine was uncaged (white circles; 10 ms, 1.5 mW) at the surface (1; 0 µm) and at 3.5 (2), 7.0 (3), and 10.5 (4) µm from the cell surface. Representative traces from a single neuron are shown. Scale bar (left), 20 µm. Scale (current; right): 500 ms, 30 pA. The color key indicates relative intensity from low (deep blue) to high (white). (**c**) The Hill equation was fitted to mean (± s.e.m.) data (n_H (Hill slope) = 2.293; R^2 = 0.9074) (n = 6 cells from 5 mice), which resulted in an estimate of 4.5 µm for the lateral distance at half-maximum amplitude (dashed lines). (**d**,**e**) Subcellular mapping of nAChRs in MHb neurons. (**d**) Representative 2PLSM image of a ChAT$^+$ MHb neuron, marked with uncaging positions (white circles; 50 ms, 2 mW) and the evoked response at each location. Scale bars, 20 µm (lower right) or 1 s, 60 pA (upper right). The color key indicates relative intensity from low (deep blue) to high (white). (**e**) Summary of position-dependent uncaging data for ChAT$^+$ MHb neurons (n = 8 cells from 5 mice) using PA-Nic (80 µM). Nicotine uncaging responses were recorded at the soma and at dendritic locations at the indicated linear distances from the soma surface. Mean values (+ s.e.m.) and individual responses (circles) are shown. P values determined by Tukey's *post hoc* test after one-way ANOVA ($F(4,69)$ = 4.3; P = 0.0036). (**f**–**i**) Interrogation of chronic-nicotine-mediated nAChR upregulation with PA-Nic. (**f**) Representative traces from one control and one chronic-nicotine-treated ChAT$^+$ MHb neuron stimulated via epi-illumination photolysis (0.12 mW mm^{-2}) for the indicated durations. Scale: 200 pA, 2 s. (**g**) The Hill equation was fitted to photochemical dose response mean values (± s.e.m.) from control (n = 7 cells from 2 mice) or chronic-nicotine-treated neurons (n = 11 cells from 3 mice) (control: n = 1.7, duration at half-maximum = 0.3 s, R^2 = 0.732; chronic nicotine: n = 1.6, duration at half-maximum = 0.3 s, R^2 = 0.89). (**h**,**i**) Chronic nicotine upregulated nAChRs at all cellular locations tested. (**h**) Representative uncaging responses from control and chronic-nicotine-treated neurons stimulated at the soma and at a dendrite ~30 µm from the soma by 405-nm laser photolysis (50 ms, 2 mW) of PA-Nic. Scale: 20 pA, 2 s. (**i**) Scatter plots (mean ± s.e.m.) of nicotine uncaging amplitudes at the indicated cellular locations for ChAT$^+$ control (n = 6 cells from 3 mice) and chronic-nicotine-treated (n = 14 cells from 4 mice) neurons. P values determined by two-sided Mann–Whitney test. Data are from n = 6 (**b**; **h**, control), 8 (**d**), 7 (**f**, control), 11 (**f**, chronic nicotine), or 14 (**h**, chronic nicotine) independent experiments.

photolysis currents were antagonized by mecamylamine and fell to noise levels with the laser spot positioned ≥10 µm from the soma (**Fig. 2a**–**c**). Currents near proximal dendrites were greater than those near distal dendrites (**Fig. 2d**,**e**). Our results showcase the temporal and spatial precision afforded by laser flash photolysis of PA-Nic.

Next, we studied the pharmacology of nAChR upregulation, a key feature of nicotine dependence. Chronic nicotine treatment upregulates nAChR function in MHb neurons[15], including neurons that express choline acetyltransferase (ChAT) (**Supplementary Fig. 4a**–**d**), but it is unknown whether this reflects an increase in the number of surface receptors or a shift in nAChR sensitivity. By generating a photochemical concentration–response curve with PA-Nic, we determined that chronic nicotine exposure increased the pharmacological efficacy of acute nicotine without affecting potency (**Fig. 2f**,**g**). This suggests that

chronic nicotine treatment increases receptor number without affecting receptor sensitivity to agonist. In laser flash recordings, uncaging responses were enhanced by chronic nicotine treatment in both somata and dendrites (**Fig. 2h**,**i**). Thus, chronic nicotine exposure induces plastic changes in postsynaptic nAChR function that may sensitize MHb neurons to cholinergic agonists, which could modulate excitability and/or dendritic integration.

We further explored PA-Nic's utility by studying nAChR-modulated excitability and Ca^{2+} mobilization. When we used a restricted field-stop aperture (**Supplementary Fig. 2k**) to constrain brief (33 ms) epi-illumination flashes (~60-µm field of view), firing was transiently enhanced when nicotine was uncaged directly over the recorded neuron, but not when nicotine was uncaged 100–200 µm away from the neuron (**Supplementary Fig. 5a**,**b**). Next, we examined Ca^{2+} dynamics in MHb $ChAT^+$ neurons expressing GCaMP6f[16] and displaying spontaneous Ca^{2+} fluctuations and responses to exogenous nicotine (**Supplementary Fig. 5c**–**e**). When we applied PA-Nic locally to the imaged neuron, perisomatic flash durations of only 5 ms (405 nm; 2 mW) were sufficient to robustly increase Ca^{2+} levels (**Supplementary Fig. 5f**,**g**). Flashes without PA-Nic were ineffective, and nAChR antagonists significantly attenuated Ca^{2+} signals induced by PA-Nic photolysis (**Supplementary Fig. 5g**,**h**). Together, these results show that PA-Nic can be used in electrophysiological or all-optical regimes for spatially delimited modulation of action potential firing or activity-dependent Ca^{2+} increases.

Finally, we examined PA-Nic's utility in other settings. MHb $ChAT^+$ neurons project to interpeduncular nucleus (IPN), where neurons are densely surrounded by cholinergic, nAChR-bearing fibers (**Supplementary Fig. 6a**,**b**). PA-Nic laser flash photolysis (2 mW; 50 ms) adjacent to IPN GABAergic neurons elicited a distinct, low-amplitude but smoldering current for which peak current versus net charge was monotonic (**Supplementary Fig. 6c**–**e**). In contrast to MHb responses, peak current and net charge did not decay with distance from the soma but were blocked by nAChR antagonists (**Supplementary Fig. 6f**–**i**). We then studied stratum radiatum interneurons in hippocampus, which express moderate levels of postsynaptic α7 nAChRs[17] (**Supplementary Fig. 6j**–**l**). Epi-illumination photolysis of PA-Nic (0.12 mW mm^{-2}; 250 ms; 2 mM PA-Nic local perfusion) efficiently activated α7, as confirmed by sensitivity to 10 nM methyllycaconitine (**Supplementary Fig. 6m**,**n**). These parameters (flash duration < 1 s, PA-Nic local perfusion, field-stop-aperture restricted) may be ideal for consistent activation of desensitization-prone nAChRs such as α7 or β2 receptors. Together, these experiments indicate that PA-Nic is broadly useful for examining nAChRs with varying kinetics and presynaptic or postsynaptic arrangements.

In summary, we have developed a flexible strategy for preparing photoactivatable derivatives of previously uncageable drugs. Our photoactivatable nicotine (PA-Nic; **9**) can be activated by relatively short-wavelength one-photon (<470 nm) or two-photon (<900 nm) light, and thus can be imaged in combination with other fluorophores or sensors. It is now possible to finely tune the spatiotemporal distribution of an nAChR agonist during optopharmacology experiments, which allows different aspects of nicotine exposure to be modeled. PA-Nic could prove useful for studying cholinergic volume versus point-to-point transmission[18], or in nAChR functional mapping[17] and imaging experiments in neurons where dendritic and/or presynaptic Ca^{2+} dynamics are rapidly modulated by nAChRs. More generally, given the number of tertiary amine compounds in the pharmacopeia, the use of a photoscissile quaternary linkage should enable the development of other photoactivatable compounds to better model drug exposure and modulate native receptor proteins in brain tissue.

METHODS

Methods, including statements of data availability and any associated accession codes and references, are available in the online version of the paper.

Note: Any Supplementary Information and Source Data files are available in the online version of the paper.

ACKNOWLEDGMENTS

We thank members of the Drenan and Lavis laboratories for helpful advice and discussion, and T. Lerner (Northwestern University, Chicago, Illinois, USA) for contributing viral reagents. This work was supported by the Howard Hughes Medical Institute (to S.B., J.J.M., and L.D.L.), the US National Institutes of Health (NIH) (grants DA035942 and DA040626 to R.M.D., MH099114 to A.C., DA037161 to H.A.L., NS054850 to D.J. Surmeier, and GM103801 and GM48677 to J.M.M.), the PhRMA Foundation (fellowship to M.C.A.), the Arnold and Mabel Beckman Foundation (Beckman Young Investigator Award to Y.K.), the Bernice E. Bumpus Foundation (Early Career Innovation Award to Y.K.), the Rita Allen Foundation (to Y.K.), the Searle Scholars Program (to Y.K.), the Alfred P. Sloan Foundation (Sloan Research Fellowship to Y.K.), NINDS (grant NINDS F32 NS103243 to N.M.B.), the JPB Foundation, and Northwestern University.

AUTHOR CONTRIBUTIONS

R.M.D., M.C.A., H.A.L., S.B., K.R.G., and L.D.L. conceived the project. M.C.A., N.M.B., D.L.W., X.-T.J., J.J.M., Y.W., C.P., G.Z., V.J.K., J.J.M., A.C., Y.K., R.M.D., S.B., and L.D.L. planned and/or executed experiments. D.L.W., Y.K., J.M.M., and K.R.G. contributed essential reagents and expertise. R.M.D., M.C.A., S.B., and L.D.L. wrote the paper with input from all other authors. R.M.D. and L.D.L. supervised all aspects of the work.

COMPETING INTERESTS

K.R.G. is an employee of Thermo Fisher Scientific and has stock options. All other authors declare no competing interests.

1. Matsuzaki, M. *et al. Nat. Neurosci.* **4**, 1086–1092 (2001).
2. Ellis-Davies, G.C. *Nat. Methods* **4**, 619–628 (2007).
3. Matsuzaki, M., Hayama, T., Kasai, H. & Ellis-Davies, G.C.R. *Nat. Chem. Biol.* **6**, 255–257 (2010).
4. Furuta, T. *et al. Proc. Natl. Acad. Sci. USA* **96**, 1193–1200 (1999).
5. Hagen, V. *et al. Angew. Chem. Int. Ed. Engl.* **44**, 7887–7891 (2005).
6. Hagen, V. *et al. Chemistry* **14**, 1621–1627 (2008).
7. Sarker, A.M., Kaneko, Y. & Neckers, D.C. *J. Photochem. Photobiol. Chem.* **117**, 67–74 (1998).
8. Petersson, E.J., Choi, A., Dahan, D.S., Lester, H.A. & Dougherty, D.A. *J. Am. Chem. Soc.* **124**, 12662–12663 (2002).
9. McCarron, S.T., Feliciano, M., Johnson, J.N. & Chambers, J.J. *Bioorg. Med. Chem. Lett.* **23**, 2395–2398 (2013).
10. Asad, N. *et al. J. Am. Chem. Soc.* **139**, 12591–12600 (2017).
11. Filevich, O., Salierno, M. & Etchenique, R. *J. Inorg. Biochem.* **104**, 1248–1251 (2010).
12. Shih, P.Y. *et al. J. Neurosci.* **34**, 9789–9802 (2014).
13. Ren, J. *et al. Neuron* **69**, 445–452 (2011).
14. Salas, R., Sturm, R., Boulter, J. & De Biasi, M. *J. Neurosci.* **29**, 3014–3018 (2009).
15. Shih, P.Y., Mcintosh, J.M. & Drenan, R.M. *Mol. Pharmacol.* **88**, 1035–1044 (2015).
16. Chen, T.W. *et al. Nature* **499**, 295–300 (2013).
17. Khiroug, L., Giniatullin, R., Klein, R.C., Fayuk, D. & Yakel, J.L. *J. Neurosci.* **23**, 9024–9031 (2003).
18. Parikh, V., Kozak, R., Martinez, V. & Sarter, M. *Neuron* **56**, 141–154 (2007).

ONLINE METHODS

Chemical synthesis and photochemistry. Experimental details, characterization for all novel compounds, and determination of photochemical byproducts of PA-Nic photolysis can be found in **Supplementary Note 1**.

UV–Vis and fluorescence spectroscopy. Spectroscopy was performed using 1-cm path length, 3.5-mL quartz cuvettes from Starna Cells or 1-cm path length, 1.0-mL quartz microcuvettes from Hellma. All measurements were taken at ambient temperature (22 ± 2 °C). Absorption spectra were recorded on a Cary Model 100 spectrometer (Agilent). Fluorescence emission spectra were recorded on a Cary Eclipse (Varian). Absolute fluorescence quantum yields were recorded on a Quantaurus-QY spectrometer (model C11374; Hamamatsu). All spectroscopy measurements were performed in phosphate-buffered saline (PBS), pH 7.4, and the values of maximum absorption wavelength (λ_{max}), extinction coefficient at λ_{max} (ε), maximum fluorescence emission wavelength (λ_{em}), and fluorescence quantum yield (Φ_f) presented are averages ($n = 3$; **Supplementary Fig. 1k**).

HPLC and LC-MS. High-performance liquid chromatography (HPLC) was performed on an Agilent 1200 Analytical HPLC system equipped with an autosampler and diode array detector. To measure the uncaging quantum yield (Φ_u; **Fig. 1c**), we monitored the loss of PA-Nic (**9**) using a 4.6 × 150 mm Kinetex C18 column (Phenomenex) with a 5–95% gradient of CH_3CN in H_2O containing constant 0.1% (v/v) TFA. To examine the release of pharmacological agents **2**–**7** and coumarin byproducts **10** and **11** from compounds **12**–**17** (**Supplementary Fig. 1**), we assessed samples by tandem liquid chromatography–mass spectrometry (LC-MS) using an Agilent 1200 LC-MS system equipped with an autosampler, diode array detector, and mass spectrometry detector using a 4.6 × 150 mm Gemini NX-C18 column with a 5–95% or 5–50% gradient of CH_3CN in H_2O containing constant 0.1% (v/v) TFA. Chromatograms were measured using absorbance at 254 nm or 210 nm, or using the total ion count, depending on the optical properties of the released drug compound.

Determination of uncaging quantum yield. Photochemistry was performed in 1-cm path length, 3.5-mL quartz cuvettes (Starna) in a Luzchem LZC 4V photoreactor equipped with 365-nm UV lamps, a carousel, and a timer as previously described[19]. Briefly, the light intensity was calibrated by potassium ferrioxalate actinometry. A solution of 60 mM $K_3Fe(C_2O_4)_3$ was irradiated using the photoreactor setup, and released Fe^{2+} was determined by complexometry with 1,10-phenanthroline. Using the known quantum yield of this process ($\Phi = 1.21$), we determined the photon flux (I) as 3.57×10^{-7} ein/min·cm^2. For the conversion of PA-Nic (**9**) to nicotine (**1**), the samples were irradiated and a small aliquot (50 µL) was placed in an amber glass high-recovery HPLC vial. These samples were analyzed by HPLC as described above. We determined Φ_u (mol/ein) by fitting a plot of HPLC peak integral signal (S) versus irradiation time to a one-phase exponential decay described by equation (1):

$$S_t = S_0 - S_0(e^{-I\sigma\Phi_u t}) \quad (1)$$

where S_0 is the signal before irradiation, t is the irradiation time (min), S_t is the signal at time t, I is the irradiation (ein/min·cm^2), and σ is a decadic extinction coefficient (in units of cm^2/mol; 1,000-fold higher than the ε value with units of M^{-1} cm^{-1} based on cuvette geometry). For the conversion of compound **9** to compound **1**, we obtained a Φ_u value of 0.74% (**Fig. 1c**). Coumarin-based cages have broad utility in the release of small-molecule modulators of biological activity[4–6,20–24]; we note that although the Φ_u value for **9** was lower than those for coumarin caged molecules that release better leaving groups such as carboxylates and phosphates[4–6,21,23], it was similar to the Φ_u value of a 7-amino-coumarin caged compound that releases an amine via a carbamate linkage[6]. For other caged compounds, the uncaging quantum yield was determined by illumination with a 405-nm LED (LOCTITE CL20 flood array), using **9** as a standard (**Supplementary Fig. 1h**, **Supplementary Note 1**).

Two-photon action cross-section for fluorescence and uncaging. We quantified the efficacy of uncaging by two-photon excitation by determining the uncaging action cross-section δ_u, which is the product of the two-photon absorption cross-section (σ_2) and the two-photon uncaging quantum yield (Φ_{2u}). In addition, as **9** is moderately fluorescent (**Supplementary Fig. 1k**), we also characterized the two-photon fluorescence action cross-section δ_f, which is the product of σ_2 and the two-photon fluorescence quantum yield (Φ_2), properties that are known for the reference dye fluorescein[25,26]. The action cross-sections δ_u and δ_f are expressed in units of Goeppert–Mayer (GM), where 1 GM is defined as 10^{-50} cm^4·s photon^{-1}. To determine δ_f we used the experimental setup previously described[27,28]; 1 µM solutions of PA-Nic (**9**) in PBS, GCaMP6f in 30 mM MOPS buffer, pH 7.2, containing 100 mM KCl and 10 mM Ca·EGTA, or reference dye fluorescein in 50 mM sodium borate buffer, pH 9.5, were illuminated in an epi-illumination microscope (IX-81, Olympus) with light from a mode-locked femtosecond Ti:Sapphire laser (Chameleon Ultra II, Coherent). Fluorescence collected by the 1.2-NA (numerical aperture) objective (UplanSApo 60× W; Olympus) was reflected off the laser dichroic (675DCSPXR; Omega Optical), spectrally filtered (539/278; Semrock), and focused by the tube lens onto a fiber-coupled avalanche photodiode (SPCM-AQRH-14-FC; Excelitas). The system was run under computer control to set both laser wavelength (700–1,080 nm) and power (1 mW at the sample plane), and to record and store the avalanche photodiode signal. The use of 1 mW of laser power focused with the 1.2-NA objective yielded sufficiently low laser intensity that no fluorescence was observed from the photolysis product compounds **10** and **11**. At each laser wavelength, the action cross-section of PA-Nic (**9**) was found from equation (2):

$$\Phi_{2S}\sigma_{2S} = \Phi_{2F}\sigma_{2F}\frac{(F(t))_S}{(F(t))_F}\frac{\eta_F}{\eta_S}\frac{T_F}{T_S} \quad (2)$$

where the subscripts S and F refer to the sample (PA-Nic or GCaMP6f) and fluorescein, respectively; Φ_2 is the two-photon fluorescence quantum yield (usually equal to the one-photon fluorescence quantum yield, Φ_f), σ_2 is the two-photon absorption cross-section in GM, $\langle F(t)\rangle$ is the fluorescence signal recorded by the detector in counts per second, η is the detector quantum efficiency averaged over the fluorescence emission spectrum, and T is the fraction of the fluorescent light transmitted through the bandpass filter. Using this equation, together with the known fluorescein two-photon absorption cross-section (average of values from refs. 25,26) and assuming Φ_{2F} is equal to the one-photon

fluorescein fluorescence quantum yield (Φ_f = 0.92), we determined the two-photon fluorescence action cross-section spectrum of PA-Nic and GCaMP6f (**Supplementary Fig. 3a**,**c**).

To determine the δ_u of PA-Nic (**9**), we adapted previously described methods[4,29] to find the fractional amount of photolysis by HPLC (Shimadzu UFLC system with diode array detector; 4.6 × 150 mm Gemini NX-C18 column with a 5–95% gradient of CH_3CN in H_2O containing constant 0.1% (v/v) TFA). Photolysis experiments proceeded as follows: laser light from a Ti:Sapphire laser was focused by a 50-mm focal-length achromatic doublet lens (AC254-050-B; Thorlabs) into a sub-micro cuvette (16.10F-Q-10; Starna) containing a solution of PA-Nic (10 µM, 18 µL) in PBS buffer. The solution also contained 50 µM 3-(4-methoxyphenyl)propan-1-amine, a non-photolyzable internal concentration standard to correct for evaporation during the illumination period, as the sealed cuvette contained an ~180-µL head volume of air. Laser power of 0.75 W was used for all photolysis experiments, measured after transmission through the cuvette. As a diagnostic, a side-observing fiber-coupled spectrometer was set up to monitor the fluorescence spectrum of the PA-Nic solution in the cuvette during excitation. This allowed observation of spurious back-scattering effects from the PA-Nic solution that interrupted laser mode-locking, evidenced by abrupt disappearance of PA-Nic fluorescence. A quarter-wave plate placed between the laser and focusing lens was found sufficient to eliminate the spurious effects on laser mode-locking. To obtain the photolysis rate, we illuminated PA-Nic samples for various time intervals from 0 to 40 min at 810 nm, 760 nm, or 720 nm and analyzed them by HPLC as described above (n = 3; **Supplementary Fig. 3b**). To obtain the spectral dependence of photolysis, we illuminated solutions of PA-Nic for 40 min at wavelengths between 710 nm and 930 nm and then analyzed them by HPLC. To determine the δ_u of PA-Nic, we again used fluorescein as an external standard, which allowed δ_u to be expressed according to equation (3)[4,29]:

$$\delta_u = \Phi_{2u}\sigma_{2S} = \frac{N_p}{\langle F(t)\rangle_F}\frac{C_F}{C_S}\Omega\Phi_{2F}\sigma_{2F} \quad (3)$$

where Φ_{2u} and σ_{2S} are the two-photon uncaging quantum yield and absorption cross-section, respectively, of PA-Nic; N_p is the rate of uncaging in molecules per second as determined by HPLC; C_S is the initial concentration of PA-Nic; C_F is the concentration of fluorescein; $\langle F(t)\rangle$ is the time-averaged rate of fluorescence (photons per second), collected by a power detector with collection efficiency Ω; and Φ_{2F} and σ_{2F} are the two-photon fluorescence quantum yield and two-photon absorption cross-section, respectively, of fluorescein. For determination of $\langle F(t)\rangle_F$, fluorescein in 50 mM sodium borate buffer, pH 9.5, was placed in a cuvette (3-Q-10; Starna) and illuminated at 810 nm, 760 nm, or 720 nm with focused laser light (0.75 W) as above, and a side-observing power meter (PM100A console, S120C head; Thorlabs) was used to record the fluorescent power produced. To eliminate scattered laser light, we placed an infrared-blocking filter (720/SP; Semrock) in front of the detector. The fraction of the total fluorescent power collected by the power meter is given by equation (4)[4]:

$$\Omega = \frac{r^2 y}{4R^2 n^2} \quad (4)$$

where r is the radius of the power meter (4.85 mm), R is the distance from the fluorescence axis to the detector face (45 mm), y is the measured filter transmission (0.97), and n is the refractive index of water (1.33). The δ_u of PA-Nic was determined to be 0.094 GM at 810 nm, 0.059 at 760 nm, and 0.025 GM at 720 nm. The value at 810 nm was used to set the scale for converting the spectrum of photolysis versus excitation to a spectrum of uncaging action cross-section, the shape of which agreed with the fluorescence action cross-section (**Supplementary Fig. 3c**), reflecting the spectral dependence of the underlying two-photon absorption cross-section.

Reagents for neurobiology experiments. QX-314, CNQX, SR16584, and D-AP5 were obtained from Tocris. RuBi-Nic was obtained from Abcam. α-conotoxin MII was synthesized as previously described[30,31]. ACh, mecamylamine (mec), atropine, picrotoxin, dihydro-β-erythroidine, and all other chemicals were obtained from Sigma unless otherwise specified.

Mice. An animal study protocol pertaining to this study (#IS00003604) was reviewed and approved by the Northwestern University Institutional Animal Care and Use Committee. Procedures also followed the guidelines for the care and use of animals provided by the National Institutes of Health Office of Laboratory Animal Welfare. Mice were housed at 22 °C on a 12-h light/dark cycle with food and water *ad libitum*. Mice were weaned on postnatal day 21 and housed with same-sex littermates. Unless stated otherwise, experiments were conducted on C57BL/6J mice obtained from Jackson Laboratories (Jax #000664). ChAT-IRES-Cre[32] (Jax #006410) (ChAT-Cre) and Ai14 (ref. 33) (Jax #007914) mouse strains were crossed to yield ChAT-Cre::Ai14 mice, which express tdTomato in a Cre-dependent manner (i.e., in neurons with an active ChAT promoter). Expression of tdTomato in MHb $ChAT^+$ neurons was confirmed in these mice via immunohistochemistry and confocal microscopy (**Supplementary Fig. 2d**). We created GAD2-Cre::Ai14 mice, which express tdTomato in $GAD2^+$ neurons, by crossing Ai14 mice to GAD2-IRES-Cre[34] (Jax #010802) (GAD2-Cre). Pre-weanling mice (<21 d old) were used for stratum radiatum recordings. All other mice used were 8–24 weeks old.

Stereotaxic injection surgery. AAV5.CAG.Flex.GCaMP6f.WPRE.SV40 vectors for Cre-dependent expression of GCaMP6f were obtained from University of Pennsylvania Vector Core (lot #V5532L, titer 1.74×10^{13} GC/mL). Male and female ChAT-Cre mice were used for surgery starting at 8 weeks of age. Mice were initially anesthetized with an intraperitoneal (i.p.) injection of a ketamine–xylazine mixture (120 mg/kg ketamine, 16 mg/kg xylazine). Mice were given additional 'boost' injections of ketamine (100 mg/kg i.p.) as needed. Alternatively, some mice were anesthetized with isoflurane: 3% (flow rate 500 mL/min) for induction and 1.5% (28 mL/min) for maintenance. Mice were secured in a stereotaxic frame and a small incision at the top of the head was made to expose the skull. Coordinates used for bilateral MHb injections were (relative to bregma, in millimeters) medial–lateral (M/L), ±0.3; anterior–posterior (A/P), −1.58; dorsal–ventral (D/V), −2.75 with overshoot to −3.0 before retraction to −2.75. Exact coordinates were adjusted to account for slight differences in head size between individual mice: the bregma/lambda

doi:10.1038/nmeth.4637

distance measured for each mouse was divided by the reported bregma/lambda distance for C57 mice (4.21), then multiplied by the A/P coordinate. The injection needle was slowly lowered through the drilled hole to the D/V coordinate. For adeno-associated viruses, 300 nL of virus (per hemisphere) was infused at a rate of 50 nL/min. The injection needle was left in place for 10 min after the infusion ended before being slowly retracted. Sutures were used to close the incision. At the conclusion of the surgery, mice were given ketoprofen (5 mg/kg by subcutaneous injection) and placed in a recovery cage, kept warm, and observed until they were ambulatory. Mice were single-housed after virus injection surgery and were given at least 14 d to recover and for the virus to express before experimental procedures were started.

Chronic nicotine treatment. Mice were treated with nicotine via drinking water as previously described[35], with minor modifications. Nicotine hydrogen tartrate or L-tartaric acid (control group) was dissolved in tap water (pH 7.0) supplemented with saccharin sodium (3 mg/mL) to mask the bitter taste of nicotine. We used the following treatment schedule (nicotine (reported as nicotine free base), tartaric acid; in μg/mL): days 1–2, (50, 75); days 3–4, (100, 150); day 5 and beyond, (200, 300). On day 5 and beyond we maintained doses by replacing drinking water solutions every 2–3 d, and mice were treated for at least 28 d before experimentation. We previously demonstrated upregulation of nAChR function in MHb VI neurons by using a different chronic nicotine exposure method: subcutaneous osmotic minipump implantation[15]. Therefore, we validated this result with the nicotine drinking water method in C57BL/6 mice (**Supplementary Fig. 4a**,**b**) before conducting PA-Nic uncaging experiments coupled with chronic nicotine studies on ChAT-Cre::Ai14 mice (**Supplementary Fig. 4c**,**d**, **Fig. 2f**–**i**).

Brain slice preparation. For epi-illumination and 405-nm laser uncaging, brain slices were prepared as previously described[36]. Mice were anesthetized with Euthasol (sodium pentobarbital, 100 mg/kg; sodium phenytoin, 12.82 mg/kg) before trans-cardiac perfusion with oxygenated (95% O_2/5% CO_2), 4 °C *N*-methyl-D-glucamine (NMDG)-based recovery solution that contained (in mM) 93 NMDG, 2.5 KCl, 1.2 NaH_2PO_4, 30 $NaHCO_3$, 20 HEPES, 25 glucose, 5 sodium ascorbate, 2 thiourea, 3 sodium pyruvate, 10 $MgSO_4{\cdot}7H_2O$, and 0.5 $CaCl_2{\cdot}2H_2O$; 300–310 mOsm, pH 7.3–7.4. Brains were immediately dissected after the perfusion and held in oxygenated, 4 °C recovery solution for 1 min before a brain block containing the MHb was cut and the brain was sectioned with a vibratome (VT1200S; Leica). Coronal slices (250 μm) were sectioned through the MHb (**Supplementary Fig. 2b**) and transferred to oxygenated, 33 °C recovery solution for 12 min. Slices were then kept in holding solution (containing, in mM, 92 NaCl, 2.5 KCl, 1.2 NaH_2PO_4, 30 $NaHCO_3$, 20 HEPES, 25 glucose, 5 sodium ascorbate, 2 thiourea, 3 sodium pyruvate, 2 $MgSO_4{\cdot}7H_2O$, and 2 $CaCl_2{\cdot}2H_2O$; 300–310 mOsm, pH 7.3–7.4) for 60 min or more before recordings. For data in **Supplementary Figure 2f** only, slices containing ventral tegmental area (~bregma −3.5 mm) were prepared.

For two-photon uncaging, brain slices were prepared as follows. Animals were deeply anesthetized by inhalation of isoflurane and decapitated, and the brain was rapidly removed and immersed in ice-cold oxygenated artificial cerebrospinal fluid (ACSF) containing (in mM) 127 NaCl, 2.5 KCl, 25 $NaHCO_3$, 1.25 NaH_2PO_4, 2.0 $CaCl_2$, 1.0 $MgCl_2$, and 25 glucose (osmolarity ~310 mOsm/L). Tissue was blocked and transferred to a slicing chamber containing ice-cold ACSF, supported by a small block of 4% agar. Bilateral 250-μm-thick slices containing the MHb were cut on a Leica VT1000S and transferred to a holding chamber with ACSF equilibrated with 95% O_2, 5% CO_2. Slices were incubated at 34 °C for 15–30 min before electrophysiological recording.

UV–Vis nicotine uncaging. Brain slices were transferred to a recording chamber while being continuously superfused at a rate of 1.5–2.0 mL/min with oxygenated 32 °C recording solution. The recording solution contained (in mM) 124 NaCl, 2.5 KCl, 1.2 NaH_2PO_4, 24 $NaHCO_3$, 12.5 glucose, 2 $MgSO_4{\cdot}7H_2O$, and 2 $CaCl_2{\cdot}2H_2O$; 300–310 mOsm, pH 7.3–7.4. Picrotoxin (100 μM), CNQX (20 μM), and D-AP5 (50 μM) were added during MHb subcellular uncaging experiments; these three drugs plus TTX (0.5 μM) were added during IPN subcellular uncaging experiments. Holding potential for voltage-clamp recordings during epi-illumination or one-photon laser flash photolysis was −60 mV, except that recordings in stratum radiatum involved pooling responses from cells held at −60 mV and −70 mV. TEA (5 mM) was added to the recording solution when the holding potential was 0 mV. Patch pipettes were pulled from borosilicate glass capillary tubes (1B150F-4; World Precision Instruments) using a programmable microelectrode puller (P-97; Sutter Instrument). Tip resistance ranged from 4.5 to 8.0 M when filled with internal solution. The following internal solution was used (in mM): 135 potassium gluconate, 5 EGTA, 0.5 $CaCl_2$, 2 $MgCl_2$, 10 HEPES, 2 MgATP, and 0.1 GTP; pH adjusted to 7.25 with Tris base; osmolarity adjusted to 290 mOsm with sucrose. For subcellular uncaging, this internal solution also contained QX-314 (2 mM) for improved voltage control. We recorded from neurons in the ventral 50–60% of the MHb, as previously described[12,15].

For epi-illumination uncaging experiments, a Nikon Eclipse FN-1 upright microscope equipped with infrared and visible differential interference contrast optics and a 40×/0.80-NA objective was used to visualize cells within brain slices. A computer running pCLAMP 10 software (Molecular Devices) was used to acquire whole-cell recordings along with an Axopatch 200B amplifier and a 16-bit Digidata 1440 A/D converter (both from Molecular Devices). Data were sampled at 10 kHz and low-pass filtered at 1 kHz. Immediately before gigaseal formation, the junction potential between the patch pipette and the superfusion medium was nulled. Series resistance was uncompensated. An LED light source (XCite 110LED; Excelitas) coupled to excitation filters (400/40 nm, 470/40 nm, and 560/40 nm bandpass) was used for photostimulation. Internal LEDs in the XCite 110LED were (center wavelength/full-width at half-maximum, in nm) 385/30, 470/40, 560/80, and 640/40. For near-UV photostimulation, flash wavelength was therefore approximately 390 ± 10 nm. Light flashes were triggered by pCLAMP via TTL pulses. Flash energy output from the LED was determined by calibration using a photodiode power sensor (Model S120C; Thor Labs).

Some experiments involved recording inward currents after pressure-ejection application of drug to the recorded cell using a drug-filled pipette, which was moved to within 20–40 μm of the recorded neuron using a micromanipulator. Using a Picospritzer (Parker Hannifin), a pressure ejection dispensed drug (dissolved

in the same superfusion medium used on the slice) onto the recorded neuron. Ejection volume, duration, and ejection pressure varied depending on whether a short (milliseconds) or long (seconds) pulse was required. The change in amplitude between the baseline and the peak was measured. Atropine (1 μM) was present in the superfusion medium when ACh was used to prevent activation of muscarinic ACh receptors. To prevent stray light from prematurely uncaging nicotine inside the drug pipette, we restricted the field stop aperture on the microscope, and retracted the drug pipette from the cell immediately after the application.

For focal nicotine uncaging using one-photon laser (405 nm) flash photolysis, an Olympus BX51 upright microscope with a 60×/1.0-NA objective was used to visualize cells. Prairie View 5 (Bruker Nano) software was used for acquisition via a Multiclamp 700B patch-clamp amplifier (Molecular Devices). Analog signals were sampled at 5 kHz and low-pass filtered at 1 kHz, and an A/D converter (PCI-NI6052e; National Instruments) was used for digitization. Patch-clamp recordings were carried out using the internal solution mentioned above, except that Alexa Fluor 568 (50 μM) or Alexa Fluor 488 (100 μM) was also included in the recording pipette to visualize cells in 2PLSM. After break-in, the internal solution with the Alexa Fluor dye was allowed to equilibrate for 15–20 min before imaging was initiated. The vast majority of 2PLSM one-photon uncaging experiments used Alexa Fluor 488 and a Mai Tai HP1040 (Spectra Physics) tuned to 900 nm, whereas several pilot studies used Alexa Fluor 568 and a Mira 900 (Coherent) infrared laser (with Verdi 10W (532-nm) pump laser) tuned to 790 nm. The laser was pulsed at 80 MHz (Mai Tai HP) or 76 MHz (Mira) (<100-fs or ~250-fs pulse duration, respectively), and a Pockels cell (ConOptics) was used for power attenuation. The dual-channel, two-photon fluorescence was detected by two non-descanned detectors; green and red channels (dual-emission filters: 525/70 nm and 595/50 nm) were detected by the following Hamamatsu photomultiplier tubes, respectively: end-on GaAsP (7422PA-40) and side-on multi-alkali (R3896). A 405-nm continuous wave laser (100 mW OBIS FP LX; Coherent) was used for photostimulation/uncaging via a second set of *x*–*y* galvanometers incorporated into the scanhead (Cambridge Technologies). A spot diameter of ~1 μm was used for all such laser flash photolysis experiments. 405-nm laser power was measured below the sample but above the condenser using a Field Master GS (LM10 HTD sensor head). A validation study on MHb neurons was conducted with the 405-nm laser in the absence of PA-Nic to identify any laser-pulse-associated artifacts (current deflections) in the voltage-clamp record. Small (<10 pA) inward currents were detected in several MHb cells when they were stimulated with 4–5 mW pulses (50 ms) but not at <2.5 mW (**Supplementary Fig. 3h**,**i**), so laser pulses in this study did not exceed 2 mW.

PA-Nic was applied (40–80 μM in 5 mL) via superfusion to the slice with a recirculating perfusion system to conserve compound. For some MHb recordings, all MHb Ca^{2+} imaging, and all hippocampus recordings, local perfusion of PA-Nic (2 mM) was used. For such studies, a glass pipette with a large diameter (20–40 μm) was back-filled with PA-Nic (2 mM) dissolved in ACSF and was connected to a pressure-ejection device. The PA-Nic-filled pipette was maneuvered to within ~50 μm of the recorded neuron, and perfusion was triggered with a constant, low pressure (1–2 p.s.i.). Prairie View 5 software was used to select spots in the field of view for focal uncaging of nicotine via 405-nm laser light flashes. Typical flash durations were 5–50 ms (unless otherwise stated), as selected after an analysis of the relationship between pulse duration and nAChR activation (**Supplementary Fig. 3l**,**m**).

Two-photon Ca^{2+} imaging with UV–Vis nicotine uncaging. MHb neurons from ChAT-Cre mice infected with AAV5.CAG.Flex.GCaMP6f.WPRE.SV40 vectors were identified by two-photon excitation of GCaMP6f (920 nm, ~250-fs pulse duration, 2–3.5 mW) with a 60×/1.0-NA objective. Time-lapse images (0.074-μm^2 pixels, 2-μs pixel dwell time, 6× optical zoom, 0.65-s sampling rate) were acquired from GCaMP6f-expressing neurons that spontaneously oscillated between high and low Ca^{2+} (**Supplementary Fig. 5d**); neurons not showing this behavior were not selected for imaging. Spontaneously active neurons (n = 5) were tested for responsiveness to nicotine via superfusion of 100 μM nicotine (**Supplementary Fig. 5e**). For time-lapse images, we quantified the changes in Ca^{2+} by calculating the mean pixel intensity along a two-dimensional (line scan) region of interest crossing the soma. For Ca^{2+} imaging experiments involving PA-Nic laser flash photolysis, PA-Nic (2 mM) was locally perfused as described above. Somatic changes in Ca^{2+} before and after PA-Nic photolysis were recorded with a continuous line scan. The GCaMP6f line-scan signal was acquired at 0.33 ms per line and 90 pixels per line with 0.08-μm pixels and 2-μs pixel dwell. Fluorescence intensity values were acquired from the soma and recorded as the mean of 11 pixels from the line scan. The line scan was initiated 5 s before the triggered laser flash (405 nm, 5 ms, 2 mW) and continued for 15 s after the light flash. Line scan data were processed with a 21-point moving average before analysis. Ca^{2+} flux was expressed as the change in fluorescence from baseline ($\Delta F/F_0$), as described in equation (5):

$$\frac{\Delta F}{F_0} = \frac{(F_p - F_0)}{F_0} \tag{5}$$

where F_0 is the baseline GCaMP6f signal, calculated as the mean signal from the 2 s before photostimulation, and ΔF is the change in fluorescence, calculated as the difference between the peak response (F_P, the mean signal from a 1-s window starting 4 s after photostimulation) and F_0.

Two-photon nicotine uncaging. Slices were transferred to a recording chamber perfused with oxygenated ACSF at a flow rate of 2–3 mL/min. Whole-cell recordings were obtained from neurons of the MHb visualized under infrared Dodt contrast video microscopy using patch pipettes of ~2–5 MΩ resistance. One internal solution consisted of (in mM) 135 $KMeSO_3$, 5 KCl, 0.5 $CaCl_2$, 5 HEPES, 5 EGTA, 10 phosphocreatine disodium salt, 2 ATP, 0.5 GTP. A second internal solution, used in mec blockade experiments, contained (in mM) 120 $CsMeSO_4$, 15 CsCl, 8 NaCl, 10 TEA-Cl, 10 HEPES, 2 QX-314, 4 ATP, 0.3 GTP, 0.2 EGTA. Alexa Fluor 488 (10–20 μM) was added to the internal solution to visualize cell morphology and confirm cell identity and location. Recordings were made with a Multiclamp 700B amplifier (Molecular Devices). Data were sampled at 10 kHz and filtered at 3 kHz, acquired in MATLAB (MathWorks). Series resistance, measured with a 5-mV hyperpolarizing pulse in voltage clamp, was under 30 MΩ and was left uncompensated. All two-photon uncaging voltage-clamp recordings were made at a holding potential

doi:10.1038/nmeth.4637

of −70 mV. ACh sensitivity, observed in 100% of recorded neurons in the experiments validating PA-Nic uncaging efficacy, was tested by pressure-ejection application of 1 mM ACh in ACSF.

2PLSM and two-photon laser photoactivation were accomplished on a modified Scientifica microscope with a 60×/1.0-NA objective. Two mode-locked Ti:Sapphire lasers (Mai-Tai eHP Deep See and Mai-Tai eHP; Spectra Physics) were separately tuned, with beam power controlled by independent Pockels cells (ConOptics). The beams were separately shuttered, recombined using a polarization-sensitive beam-splitting cube (Thorlabs), and guided into the same galvanometer scanhead (Cambridge). The Mai Tai eHP Deep See was tuned to 910 nm for excitation of Alexa Fluor 488, and the Mai Tai eHP was variably tuned between 690 and 1,000 nm to uncage PA-Nic. A modified version of ScanImage was used for data acquisition[37]. PA-Nic was added by superfusion (100 µM) or via pressure ejection. For PA-Nic pressure ejection, 300-ms pulses of 200 µM solution in ACSF were delivered at 5–10 p.s.i. through a patch pipette placed 20–60 µm away from the recorded cell. Successful photoactivation of PA-Nic, confirmed by blockade with mec (pre-mec, 11.06 ± 0.9 pA; post-mec, 8.56 ± 1.2 pA; n = 11; P = 0.008, paired t-test), was observed at the following parameter ranges: 3–20-ms pulse widths, 680–880-nm uncaging laser tuning, and 10–80-mW power measured at the sample plane. A spot diameter of ≤0.8 µm, based on measurements of 0.5-µm beads (17152-10; Polysciences Inc.) imaged with the uncaging laser, was used for all two-photon laser flash photolysis experiments. Two GaAsP photosensors (Hamamatsu, H7422) with 520/28-nm bandpass filters (Semrock), mounted above and below the sample, were used to image Alexa Fluor 488 fluorescence signals.

Immunohistochemistry and confocal microscopy. Mice were anesthetized with sodium pentobarbital (100 mg/kg i.p.) and transcardially perfused with 10 mL of heparin-containing PBS followed by 30 mL of 4% paraformaldehyde. Brains were dissected, postfixed in 4% paraformaldehyde overnight at 4 °C, and dehydrated in 30% sucrose. Coronal brain slices (50 µm) were cut on a freezing/sliding microtome (SM2010R; Leica). For staining of MHb-containing slices, slices were first permeabilized for 2 min via incubation in PBST (0.3% Triton X-100 in PBS), and then incubated for 60 min in blocking solution (0.1% Triton X-100, 5% horse serum in Tris-buffered saline (TBS)). Primary antibodies used in this study were as follows: goat anti-ChAT (Millipore; AB144P), rabbit anti-DsRed (Clontech; 632496). Primary antibodies were diluted in blocking solution (anti-ChAT at 1:100, anti-DsRed at 1:500). Slices were incubated in primary antibodies overnight at 4 °C. Three 5-min washes in TBST (0.1% Triton X-100 in TBS) were done before slices were transferred to secondary antibodies for a 60-min incubation at room temperature. Secondary antibodies, diluted 1:500 in blocking solution, were as follows: anti-goat Alexa Fluor 488 (Invitrogen; A11055), anti-rabbit Alexa Fluor 647 (Invitrogen; A31573). Slices were washed as before, mounted on slides, and coverslipped with Vectashield. Staining in the MHb or IPN was imaged as previously described[12] with a Nikon A1 laser-scanning confocal microscope.

Statistics and data analysis. For spectroscopy and photolysis experiments, n denotes the number of independent samples tested, typically prepared from a singular stock solution in DMSO or water. For biology experiments, two-sided statistical tests were done with GraphPad Prism 6 software. Flash photolysis responses in IPN were analyzed in MATLAB; for these recordings only, peak inward current was defined as the maximum change in current responses within 100 ms of laser flash onset. For all other laser flash photolysis recordings, the peak current occurred at ±200 ms of laser flash offset. For pharmacological experiments involving animal models, sample sizes were selected on the basis of prior similar studies[12,15], and mice of the appropriate age (2–24 weeks) were randomly (informal randomization) chosen for assignment to specific experimental groups. For some studies involving recordings from neurons derived from mice treated with nicotine or control drinking water, the experimenter was blind to the treatment during data collection. Typically, multiple slices were cut from each brain, and often multiple samples (neurons) were analyzed within each slice depending on the experimental design requirements. During superfusion of brain slices with pharmacological agents such as receptor antagonists, slices were discarded at the conclusion of each recording. For experiments involving variations in flash strength, pulse duration, etc., it was possible to record multiple data points from the same neuron. All experiments involved a minimum of two independent replicates. Where samples were taken from animals, every reasonable effort was made to replicate findings in more than one animal. Outlier data points were removed from data sets via the ROUT method (Q = 1%) as previously described[38]. P values for **Supplementary Figures 3f** and **5b** were corrected for multiple comparisons. For presentation purposes in figures, most electrophysiology traces were downsampled to a final sampling interval of 1–2.5 ms, baseline-adjusted such that pre-stimulation current/voltage levels were approximately zero, and filtered with a moving average smoothing filter. Group sizes involving recordings from neurons in mouse brain slices are presented as number of cells/number of mice. Unless otherwise stated and where applicable, summary data are shown as mean and s.e.m.

Life Sciences Reporting Summary. Further information on experimental design is available in the **Life Sciences Reporting Summary**.

Data availability. The data that support the findings of this study, if not explicitly contained within the text, supplementary figures, or **Supplementary Note 1**, are available from the corresponding authors upon reasonable request. Source data for **Figures 1** and **2** and **Supplementary Figures 1–6** are available online.

19. Grimm, J.B. *et al. Nat. Methods* **13**, 985–988 (2016).
20. Schoenleber, R.O. & Giese, B. *Synlett.* 501–504 (2003).
21. Shembekar, V.R., Chen, Y., Carpenter, B.K. & Hess, G.P. *Biochemistry* **46**, 5479–5484 (2007).
22. Schaal, J. *et al. ChemBioChem* **13**, 1458–1464 (2012).
23. Herbivo, C., Omran, Z., Revol, J., Javot, H. & Specht, A. *ChemBioChem* **14**, 2277–2283 (2013).
24. Nadler, A. *et al. Nat. Commun.* **6**, 10056 (2015).
25. Xu, C. & Webb, W.W. *J. Opt. Soc. Am. B* **13**, 481–491 (1996).
26. Makarov, N.S., Drobizhev, M. & Rebane, A. *Opt. Express* **16**, 4029–4047 (2008).
27. Mütze, J. *et al. Biophys. J.* **102**, 934–944 (2012).
28. Grimm, J.B. *et al. Nat. Methods* **12**, 244–250 (2015).
29. Davis, M.J. *et al. J. Org. Chem.* **74**, 1721–1729 (2009).

30. Azam, L. *et al. J. Biol. Chem.* **280**, 80–87 (2005).
31. Azam, L. *et al. FASEB J.* **24**, 5113–5123 (2010).
32. Rossi, J. *et al. Cell Metab.* **13**, 195–204 (2011).
33. Madisen, L. *et al. Nat. Neurosci.* **13**, 133–140 (2010).
34. Taniguchi, H. *et al. Neuron* **71**, 995–1013 (2011).
35. Zhao-Shea, R. *et al. Nat. Commun.* **6**, 6770 (2015).
36. Engle, S.E., Broderick, H.J. & Drenan, R.M. *J. Vis. Exp.* **68**, e50034 (2012).
37. Pologruto, T.A., Sabatini, B.L. & Svoboda, K. *Biomed. Eng. Online* **2**, 13 (2003).
38. Motulsky, H.J. & Brown, R.E. *BMC Bioinformatics* **7**, 123 (2006).

doi:10.1038/nmeth.4637

nature research

Corresponding author(s): Ryan M. Drenan, Luke D. Lavis

Life Sciences Reporting Summary

Nature Research wishes to improve the reproducibility of the work that we publish. This form is intended for publication with all accepted life science papers and provides structure for consistency and transparency in reporting. Every life science submission will use this form; some list items might not apply to an individual manuscript, but all fields must be completed for clarity.

For further information on the points included in this form, see Reporting Life Sciences Research. For further information on Nature Research policies, including our data availability policy, see Authors & Referees and the Editorial Policy Checklist.

Please do not complete any field with "not applicable" or n/a. Refer to the help text for what text to use if an item is not relevant to your study.

For final submission: please carefully check your responses for accuracy; you will not be able to make changes later.

Experimental design

1. Sample size

Describe how sample size was determined.

Due to the absolute novelty of PA-Nic, sample sizes were not determined prior to experimentation. We were guided by prior studies, cited in the Online Methods, for sample size expectations.

2. Data exclusions

Describe any data exclusions.

Outlier data points were removed (rarely) via the ROUT method as described in the Online Methods.

3. Replication

Describe the measures taken to verify the reproducibility of the experimental findings.

All experiments were independently replicated. Where samples were taken from animals, every reasonable effort was made to replicate findings in more than one animal.

4. Randomization

Describe how samples/organisms/participants were allocated into experimental groups.

Where applicable, animals were randomly assigned to experimental groups via informal randomization.

5. Blinding

Describe whether the investigators were blinded to group allocation during data collection and/or analysis.

For chronic nicotine treatments, investigators performing recordings were blind to the treatment during the first ~50% of data collection to assure unbiased results.

Note: all in vivo studies must report how sample size was determined and whether blinding and randomization were used.

6. Statistical parameters

For all figures and tables that use statistical methods, confirm that the following items are present in relevant figure legends (or in the Methods section if additional space is needed).

n/a	Confirmed
☐	☒ The exact sample size (*n*) for each experimental group/condition, given as a discrete number and unit of measurement (animals, litters, cultures, etc.)
☐	☒ A description of how samples were collected, noting whether measurements were taken from distinct samples or whether the same sample was measured repeatedly
☐	☒ A statement indicating how many times each experiment was replicated
☐	☒ The statistical test(s) used and whether they are one- or two-sided *Only common tests should be described solely by name; describe more complex techniques in the Methods section.*
☐	☒ A description of any assumptions or corrections, such as an adjustment for multiple comparisons
☐	☒ Test values indicating whether an effect is present *Provide confidence intervals or give results of significance tests (e.g. P values) as exact values whenever appropriate and with effect sizes noted.*
☐	☒ A clear description of statistics including central tendency (e.g. median, mean) and variation (e.g. standard deviation, interquartile range)
☐	☒ Clearly defined error bars in all relevant figure captions (with explicit mention of central tendency and variation)

See the web collection on statistics for biologists for further resources and guidance.

Nature Methods: doi:10.1038/nmeth.4637

Software

Policy information about availability of computer code

7. Software

Describe the software used to analyze the data in this study.	Standard commercial software: MS Excel, GraphPad Prism, OriginLab, Clampfit, pClamp 10, MATLAB, PrairieView 5

For manuscripts utilizing custom algorithms or software that are central to the paper but not yet described in the published literature, software must be made available to editors and reviewers upon request. We strongly encourage code deposition in a community repository (e.g. GitHub). *Nature Methods* guidance for providing algorithms and software for publication provides further information on this topic.

Materials and reagents

Policy information about availability of materials

8. Materials availability

Indicate whether there are restrictions on availability of unique materials or if these materials are only available for distribution by a third party.	All reagents and materials are available from the authors upon reasonable request.

9. Antibodies

Describe the antibodies used and how they were validated for use in the system under study (i.e. assay and species).	goat anti-ChAT (Millipore; cat# AB144P; clone n/a; lot 2843074) rabbit anti-DsRed (Clontech; cat# 632496; clone n/a; lot not available) anti-goat Alexa 488 (Invitrogen; cat# A11055; clone n/a; lot 1827671) anti-rabbit Alexa 647 (Invitrogen; cat# A31573; clone n/a; lot 1826679) Validation: Supplementary Figure 2d: anti-ChAT and anti-DsRed staining cross-validate each other since their signals should overlap in medial habenula of ChAT-Cre::Ai14 mice. Supplementary Figure 6c: anti-DsRed staining simply increased the signal from the endogenous tdTomato expressed specifically in GAD2 neurons in IPN.

10. Eukaryotic cell lines

a. State the source of each eukaryotic cell line used.	no cell lines were used in this study
b. Describe the method of cell line authentication used.	no cell lines were used in this study
c. Report whether the cell lines were tested for mycoplasma contamination.	no cell lines were used in this study
d. If any of the cell lines used are listed in the database of commonly misidentified cell lines maintained by ICLAC, provide a scientific rationale for their use.	no cell lines were used in this study

Animals and human research participants

Policy information about studies involving animals; when reporting animal research, follow the ARRIVE guidelines

11. Description of research animals

Provide all relevant details on animals and/or animal-derived materials used in the study.	species: mus musculus strain: C57BL/6 (Jackson Labs strain numbers 000664, 006410, 007914, 010802) sex: male and female age: 2 to 24 weeks old

Policy information about studies involving human research participants

12. Description of human research participants

Describe the covariate-relevant population characteristics of the human research participants.	this study did not involve human research participants

Nature Methods: doi:10.1038/nmeth.4637